Archives of Hydro-Engineering and Environmental Mechanics 71 (2024), pp. 1–26, doi: 10.2478/heem-2024-0001

sciendo

ARCHIVES OF HYDRO-ENGINEERING AND ENVIRONMENTAL MECHANICS

Published since 1954

ISSN 1231–3726

Numerical Modeling of Sediment Transport and Bed Evolution in Nonuniform Open-Channel Flows

Yebegaeshet T. Zerihun

David & James – Engineering and Environmental Consultancy, 204 Albion Road, Vic 3350, Australia;
e-mail: zyebegaeshet@gmail.com

(Received 14 November 2023; revised 11 January 2024)

Abstract. The shallow-water and multilayer hydrostatic models have been commonly used to analyze the problems of a sediment-laden, plane open-channel flow. The models are adequate to solve a quasi-hydrostatic flow problem, but their accuracy deteriorates as the effects of the vertical acceleration gain in significance. Herein, a higher-order numerical model for treating the problems of unsteady, plane open-channel flow over a movable bed is proposed. In this model, the flow hydrodynamics is governed by the depth-averaged Boussinesq-type equations, and the bed morphodynamics is determined by an Exner-type equation and additional equations describing the non-equilibrium transports of suspended load and bed load. A hybrid finite-volume and finite-difference scheme was used to discretize and solve the governing equations, yielding solutions that are in satisfactory agreement with the experimental data. Overall, the results of the proposed model for the temporal free-surface profile and bed evolution were fairly adequate. For the two particular cases considered, however, the quality of its results was moderately affected by the effects of the three-dimensional characteristics of the dam-break flow and the sliding of the dike body due to sub-surface flow. The results of this investigation highlight the importance of including a higher-order Boussinesq-type correction for refining sediment transport computations.

Key words: turbulent flow, sediment transport, dike breach, finite-volume method, non-equilibrium transport, morphodynamics

1. Introduction

For over a century, characterizing and predicting sediment transport in open channels have been the primary issues of many research works. Numerically- and experimentally-based methods of investigation have been utilized by such works to evaluate the evolution of sediment load in open channels, and their results were effectively applied to develop design guidelines for major hydraulic infrastructures. The experimental method provides valuable insights into the basic physical processes influencing sediment transport. These processes are mostly masked or disrupted in the field by the complexities of natural fluvial systems. In addition, the temporal and spatial variations

of sediment transport make the field assessment work more difficult. A higher-order numerical model is a cost-effective alternative approach for providing a better solution to the problem of the alluvial processes involving sediment transport. It can also be used for a comprehensive study of flow-sediment interactions in a reservoir and estimation of the reservoir's storage capacity depletion rate (Zerihun 2023). The development of such a type of model is the main task of this investigation.

In recent years, several numerical models for simulating sediment transport and the variation of channel bed level have been proposed. For flow with low sediment concentration, the one-dimensional (1D) shallow-water equations for the hydrodynamics of clear-water flow over a movable bed and the sediment transport equations for the morphodynamics were linked together to develop numerical models (e.g., Capart and Young 1998, Guo and Jin 1999, El Kadi Abderrezzak and Paquier 2009, Franzini and Soares-Frazão 2018). An alternative approach, which considered a non-equilibrium sediment transport and the effects of sediment concentration on flow dynamics, was proposed by Cao et al (2004) and Wu and Wang (2008). Similar to the Guo and Jin (1999) model, the model of Cao et al (2004) is limited to analyze only suspended-load transport. Using a two-phase flow approach, Pontillo et al (2010) presented a numerical model for simulating the dike surface erosion due to overtopping flow. Xia et al (2010) also proposed a numerical model, which solved the shallow-water and non-equilibrium sediment transport equations using the finite-volume method. All these models were developed based on the restrictive assumption of a hydrostatic pressure distribution; hence, they are not suitable to model rapidly-varied flows over movable beds. For such types of flows, Zerihun (2004, p. 265) suggested the use of a coupled set of Boussinesq-type momentum and non-equilibrium sediment transport equations.

Many investigators (e.g., Berger 1992, Steffler and Jin 1993, Zerihun and Fenton 2006, Zerihun 2021) proposed full formulations of the hydrodynamic equations of a non-hydrostatic open-channel flow rather than resorting to the shallow-water theory. In comparison with the two-dimensional (2D) vertical plane flows in rigid-bed channels, the simulations of such types of flows over movable beds are more challenging due to the temporal and spatial variations of the sediment concentration and channel bed profile. As a result, such higher-order models are seldom used to study fluvial processes. For studying the transport of suspended sediment in non-uniform flows, van Rijn (1986) employed a 2D model that accounts for the effects of the vertical acceleration. Additionally, the 1D and 2D vertically averaged and moment (VAM) models (Steffler and Jin 1993, Ghamry 1999) were coupled with a bed-load transport model to simulate the geomorphic features of an open channel (Elgamal and Steffler 2001, Vasquez et al 2011). Recently, the 1D VAM approach for sediment transport (Elgamal and Steffler 2001) was enhanced to include a suspended-load transport module (Cantero-Chinchilla et al 2019). Likewise, Marsooli and Wu (2015) extended the three-dimensional (3D) Reynolds-averaged Navier-Stokes (RANS) equations by integrating the flow equations with the non-equilibrium sediment transport model,

which was originally introduced by Wu et al (2000) and Wu and Wang (2007). Although a 3D model is computationally too expensive for most practical applications, the complex features of the fluid-sediment mixture flow can be accurately mimicked by this model. In order to reduce the computational time of large-scale problems, 2D multilayer hydrostatic models were proposed for sediment transport studies (e.g., Wai et al 1996, Ramirez-León et al 2005, Rowan 2019). These models relaxed the assumption of constant horizontal velocities across the flow depth, so that they adequately capture the 3D characteristics of the shallow-water flow. The outcome of this review highlights that compared to numerical models for flow in a rigid-bed channel, very little effort has been made so far to incorporate the effects of non-uniform velocity and non-hydrostatic pressure distributions into the hydrodynamic and sediment transport models.

In this study, a higher-order numerical model, which couples an open-channel flow model with sediment transport equations, is proposed. The hydrodynamic model of the fluid-sediment mixture flow is the depth-averaged Boussinesq-type equations, which are developed based on the pre-assumed distributions of horizontal velocity and non-hydrostatic pressure. Unlike the previous Boussinesq-type momentum equations (e.g., Boussinesq 1877, Zerihun 2004, 2021), the proposed equations do not incorporate second- and third-order derivative terms of the bed profile. Consequently, the variations of the channel bed profile due to deposition and erosion can be easily simulated without the problem of numerical instability. For accurately determining the evolution of the bed levels, the non-equilibrium transport equations of suspended load and bed load are employed. It is worth emphasizing that the numerical model proposed here deals only with the transport of non-cohesive sediment. The model's capabilities for simulating morphodynamic processes are tested by considering different cases of non-uniform open-channel flows. The results are verified using available experimental data, thus allowing us to examine the impacts of the applied higher-order approximations for the vertical distributions of velocity and pressure. The use of the dynamic correction for the effects of a non-hydrostatic pressure distribution may not always be essential; it can add unnecessary complexity to the model. For a nearly hydrostatic flow situation, the proposed model can be adjusted by simply changing the values of few parameters, thereby reducing the computational effort and time. In subsequent sections, the development of the governing equations and numerical solution procedures and the validations of the numerical results are presented.

2. Mathematical Model

2.1. Hydrodynamic Equations

Figure 1 illustrates the definition sketch of a plane open-channel flow over an erodible bed. A Cartesian coordinate system, with the x axis longitudinal, y axis transversal, and the z axis vertical upward, is also shown in this figure. The transport of the fluid-sediment mixture is numerically modeled by dividing the mixture flow into

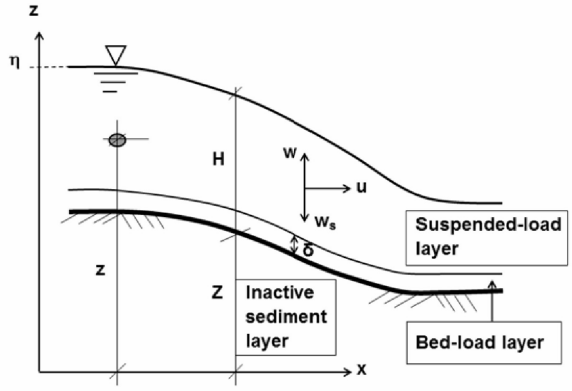

Fig. 1. Definition sketch of turbulent open-channel flow over a movable bed

suspended-load and bed-load layers. For a 2D vertical plane flow where flow variables vary both in space (only in the x- and z-directions) and time, the continuity and the RANS momentum equations (Reynolds 1895) in the conservative form can be written as follows (Vreugdenhil 1994, pp. 15–16, Schlichting and Gersten 2017, p. 505):

$$\frac{\partial}{\partial t}(\rho) + \frac{\partial}{\partial x}(\rho u) + \frac{\partial}{\partial z}(\rho w) = 0, \tag{1}$$

$$\frac{\partial}{\partial t}(\rho u) + \frac{\partial}{\partial x}\left(\rho u^2 + p - \sigma_x\right) + \frac{\partial}{\partial z}(\rho u w) - \frac{\partial}{\partial z}(\tau_{xz}) = 0, \tag{2}$$

$$\frac{\partial}{\partial t}(\rho w) + \frac{\partial}{\partial x}(\rho u w) + \frac{\partial}{\partial z}(\rho w^2 + p - \sigma_z) - \frac{\partial}{\partial x}(\tau_{zx}) + \rho g = 0, \tag{3}$$

where u and w denote the horizontal and vertical velocity components, respectively; g is acceleration due to gravity; ρ is the density of the fluid-sediment mixture; p is the pressure; σ and τ refer to the total normal and shear stresses, respectively; and t is the time. In the above equations, the density may vary in the horizontal direction, but it is assumed constant across the depth. In terms of volumetric concentration, ρ may be expressed as

$$\rho = \rho_w\left(1 - \overline{C}_T\right) + \rho_s \overline{C}_T, \tag{4}$$

where ρ_w and ρ_s are the densities of water and sediment, respectively, and $\overline{C}_T$ is the vertically-averaged total sediment concentration.

The distribution of the horizontal velocity across the flow depth is approximated by a linear relation (Zerihun 2021) as follows:

$$u = \frac{q}{H}\left(2\Lambda(1-\omega) + \omega\right), \tag{5a}$$

$$\Lambda = \frac{z - Z}{\eta - Z}, \tag{5b}$$

where q is the unit discharge; η is the free-surface elevation; Λ is a dimensionless vertical coordinate; z is the vertical elevation of a point in the flow field; Z is the channel bed elevation; H is the local flow depth; and ω is the velocity distribution parameter and tends to vary only in the x-direction. By applying Leibnitz's rule, the vertical integration of Equation (1) becomes

$$\begin{aligned}&\int_z^\eta \frac{\partial}{\partial t}(\rho)dz + \int_z^\eta \frac{\partial}{\partial x}(\rho u)dz + \int_z^\eta \frac{\partial}{\partial z}(\rho w)dz \\ &= \frac{\partial}{\partial t}(\rho) + \frac{\partial}{\partial x}\int_z^\eta (\rho u)dz + (\rho u)z_x - (\rho u_H)\eta_x + \rho w_H - \rho w = 0.\end{aligned} \tag{6}$$

Inserting Equation (4) into Equation (6) and applying the free-surface kinematic boundary condition, $w_H = \eta_t + u_H\eta_x$, results in the following expression for the vertical velocity distribution:

$$\begin{aligned}w \cong\ & H_t\left(1-\omega\left(1-\Lambda\right)-\left(1-\omega\right)\left(1-\Lambda^2\right)\right) + Z_t + \frac{q\eta_x}{H}(2-\omega) \\ & -\frac{2qZ_x}{H}\left(\left(1-\omega\right)\left(1-\Lambda\right)\right) - \frac{qH_x}{H}\left(\left(1-\Lambda\right)\omega\right) \\ & -\frac{2qH_x}{H}\left(\left(1-\omega\right)\left(1-\Lambda^2\right)\right),\end{aligned} \tag{7}$$

where u_H and w_H are the horizontal and vertical components of the velocity, respectively, at the free surface. In the above equations, the subscripts x and t denote partial differentiations with respect to the horizontal axis and time, respectively.

After decomposing the total pressure into the hydrostatic and dynamic components, a linear distribution shape for the dynamic pressure component (Jin and Li 1996) is proposed. As noted by Zerihun (2004, 2016), such a linear-type pressure equation can provide reasonably good results for a moderately curved open-channel flow problem. With this, the vertical profile of the total pressure can be expressed as

$$p = \left(\rho g H + p_D\right)\left(1-\Lambda\right), \tag{8}$$

where p_D is the dynamic pressure at the channel bed and varies only in the x-direction. It incorporates terms that account for the effects of a hydraulically steep slope.

In order to describe the local characteristics of the mixture flow in terms of the flow depth and discharge, the continuity equation and the RANS momentum equations are vertically integrated from the bed to the free surface using Equations (5a), (7) and (8). As noted by van Rijn (1984a, 1986), the thickness of the bed-load layer (δ) varies from $0.01H$ to $0.05H$, which is very small compared to H. Therefore, the depth averaging procedure is performed by ignoring the thickness of this layer and applying the following kinematic and dynamic boundary conditions:

$$p(\eta) = 0, \quad \sigma(\eta) = 0, \quad \tau(\eta) = 0, \tag{9a}$$

$$w(Z) = u(Z)Z_x + Z_t, \tag{9b}$$

$$u(Z) = 0, \tag{9c}$$

$$\tau(Z) = \tau_b. \tag{9d}$$

Equation (9b) considers the effect of the temporal variation of the channel bed on the vertical velocity. For a sediment-laden flow in a rectangular channel, the resulting vertically-averaged equations can be written as

$$\frac{\partial H}{\partial t} + \frac{\partial q}{\partial x} = -\frac{1}{\rho}\left(q\frac{\partial \rho}{\partial x} + H\frac{\partial \rho}{\partial t}\right), \tag{10}$$

$$\begin{aligned}&\frac{\partial}{\partial t}(\rho q) + \frac{\partial}{\partial x}\left(\frac{\rho q^2}{3H}\beta_1 + \frac{\rho g H^2}{2}\right) - \frac{\partial}{\partial x}\left(H\overline{\sigma}_x\right)\\ &+ (\rho g H + p_D)Z_x + \frac{\partial}{\partial x}\left(\frac{H p_D}{2}\right) + \tau_b = 0,\end{aligned} \tag{11}$$

$$\begin{aligned}&\frac{\partial}{\partial t}\left(\rho q\left(\beta_4 H_x + Z_x\right) + \rho H\left(\beta_3 H_t + Z_t\right)\right)\\ &+ \frac{\partial}{\partial x}\left(\rho\left(\frac{q^2}{H}\left[\beta_2 H_x + \beta_1 Z_x\right]\right) + \rho\left(\frac{q}{2}H_t + qZ_t\right)\right)\\ &- \frac{\partial}{\partial x}\left(H\overline{\tau}_{zx}\right) - p_D + \tau_b Z_x = 0,\end{aligned} \tag{12}$$

where τ_b is the bed shear stress; $\overline{\sigma}_x$ and $\overline{\tau}_{zx}$ are the vertically-averaged normal and tangential stresses, respectively; $\beta_1 = (\omega^2 - 2\omega + 4)/3$; $\beta_2 = (\omega^2 - 4\omega + 6)/6$; $\beta_3 = (\omega + 2)/6$; and $\beta_4 = (4 - \omega)/6$. Unlike the previous equations introduced by Jin and Li (1996), Equations (11) and (12) provide the nodal values of the dynamic bed pressure as part of the solutions to the problem. Compared to those equations for single-phase clear-water flows, the effect of sediment transport phenomenon is taken into account by the parameters $\rho(x, t)$ and $Z(x, t)$. The bed shear stress is calculated from the Manning equation as

$$\frac{\tau_b}{\rho} = \frac{g n^2 q^2}{R^{1/3} H^2}\left(1 + Z_x^2\right), \tag{13}$$

where n is the Manning roughness coefficient, which is computed by the Karim (1995) formula for a movable bed channel, and R is the hydraulic radius of a normal section. The additional terms of the turbulent stress in Equations (11) and (12) require a turbulence closure model, which will be discussed in the next section.

2.2. Model for Turbulence Effects

The simplest method to explicitly account for the effects of flow turbulence is the use of an algebraic turbulence model based on the Boussinesq eddy-viscosity hypothesis. This turbulence model is easy to implement and, with careful application, can provide

practically good results for turbulent open-channel flow problems (Ferziger and Peric 2002, p. 294). Ignoring the effects of sediment suspension, the vertically-averaged normal and tangential stresses appearing in Equations (11) and (12) are deduced from the Boussinesq (1877) equation as follows:

$$H\bar{\sigma}_x = \int_Z^\eta \sigma_x dz = 2\rho\,(\nu_m + \bar{\nu}_x)\left(q_x - \frac{q}{H}(2-\omega)\eta_x\right), \tag{14}$$

$$\begin{aligned} H\bar{\tau}_{zx} &= \int_Z^\eta \tau_{zx} dz \\ &= \rho\,(\nu_m + \bar{\nu}_z)\left(\frac{\partial}{\partial x}\left(q\left[\beta_4 H_x + Z_x\right] + H\left[\beta_3 H_t + Z_t\right]\right) + \frac{q}{H}(2-\omega)\eta_x\right), \end{aligned} \tag{15}$$

where $\bar{\nu}_x$ and $\bar{\nu}_z$ are the vertically-averaged kinematic eddy viscosities in the horizontal and vertical directions, respectively, and ν_m is the molecular kinematic viscosity. The above expressions for the turbulent stresses are added to the governing equations as source terms; they must be accurately estimated by the numerical model. The expressions for the kinematic eddy viscosity are obtained by vertically averaging the parabolic eddy-viscosity equation (Fischer et al 1979, pp. 106–107) and are given by

$$\bar{\nu}_x = \alpha_t U_\tau H, \tag{16a}$$

$$\bar{\nu}_z = C_s k U_\tau H, \tag{16b}$$

$$U_\tau = \sqrt{\frac{\tau_b}{\rho}}, \tag{16c}$$

where $C_s = 1/6$; k is the von Kármán constant; U_τ is the boundary shear velocity; and α_t is an empirical coefficient, having values in the range of 0.08 to 0.9 (Fischer et al 1979, p. 112). Equations (14)–(16) are numerically coupled with Equations (11) and (12) for the complete solutions of the sediment-laden, turbulent flow problems with curvilinear streamlines.

2.3. Sediment Transport Equations

The temporal and spatial variations of the concentration of suspended sediment in a water column are governed by the mass-balance equation. Ignoring the longitudinal diffusive transport, which is small compared to the vertical one, the sediment transport equation for a 2D vertical plane flow can be written as follows:

$$\frac{\partial c}{\partial t} + \frac{\partial}{\partial x}(uc) + \frac{\partial}{\partial z}\left((w - w_s)c\right) - \frac{\partial}{\partial z}\left(\xi_s \frac{\partial c}{\partial z}\right) = 0, \tag{17}$$

where c is the suspended sediment concentration; w_s is the settling velocity of the turbulent suspension; and ξ_s is the dispersion coefficient of the sediment in the z-direction. The vertical distribution of the suspended sediment is approximated by the following equation:

$$c = c_0 \left(1 + (1 - 2\Lambda + \Gamma_1)\,\Gamma_2\right), \tag{18a}$$

$$\Gamma_1 = \frac{(1-\omega)}{3}, \tag{18b}$$

$$\Gamma_2 = \frac{(1-\mu)}{(\Gamma_1(\mu-1)-1)}, \tag{18c}$$

where c_0 is the flux-averaged suspended sediment concentration, and μ is a coefficient determined from the following expression (Lin 1984):

$$\mu = 3.25 + 0.55\left(\ln\left(\frac{w_s}{kU_\tau}\right)\right). \tag{19}$$

In Equation (18a), the maximum value of μ is limited to $(1 - \lambda_p)/\varepsilon$, where λ_p is the porosity of the bed material, and $\varepsilon = c_0(1 + \Gamma_1\Gamma_2)$. At the free surface, the net vertical sediment flux is zero. This sediment boundary condition is mathematically expressed as

$$\left(cw_s + \xi_s \frac{\partial c}{\partial z}\right)_{z=\eta} = 0. \tag{20}$$

The dispersion coefficient appearing in Equation (17) for the solid phase is different from the eddy-viscosity coefficient appearing in Equation (14) or (15) for the turbulent transfer of momentum, except for the case of mixture flow with very small particles with low density (Bechteler and Schrimpf 1984, van Rijn 1986). Additionally, the distribution shape of the dispersion coefficient does not significantly affect the settling of suspended sediment (Bechteler and Schrimpf 1988). Using this fact and considering the sediment concentration effect, Equation (16b) is modified to give (van Rijn 1984b)

$$\xi_s = \Gamma_3 \bar{\nu}_z = \Gamma_3 C_s k U_\tau H, \tag{21}$$

where Γ_3 is a correction factor. As noted by van Rijn (1984b, 1986), this factor accounts for the difference in the diffusion of a discrete sediment particle and a fluid particle and also expresses the damping of turbulence by sediment particles.

By integrating Equation (17) over the flow depth with the use of Leibnitz's rule and application of flow and sediment boundary conditions, the vertically-averaged sediment transport equation is developed. That is,

$$\frac{\partial}{\partial t}\left(Hc_0\left(1 + \Gamma_1\Gamma_2\right)\right) + \frac{\partial}{\partial x}(qc_0) + \bar{w}_s c_0\left(1 + (1 + \Gamma_1)\,\Gamma_2\right) - \frac{\Gamma_2\Gamma_3}{3}(kU_\tau c_0) = 0, \tag{22}$$

where $\overline{w}_s$ is the vertically-averaged settling velocity. The evolution of the channel bed level is also governed by the mass-balance equation for sediment routing. By accounting for the spatial lag effect (Daubert and Lebreton 1967, Bennett 1974), Equation (17) is integrated over the depth to yield

$$\frac{\partial Z}{\partial t} = \frac{-1}{(1-\lambda_p)}\left(\frac{\partial}{\partial t}\left(Hc_0\left[1+\Gamma_1\Gamma_2\right]\right) + \frac{\partial}{\partial x}(qc_0) + \frac{q_{bE}-q_b}{L_b}\right), \tag{23}$$

where L_b is the non-equilibrium adaptation length of bed-load transport and can be estimated by the van Rijn (1984a) empirical relations; q_b is the volumetric rate of bed-load transport per unit width; and q_{bE} is the bed-load transport capacity. In the case of open-channel flows where the sediment in suspension does not significantly change over time, Equation (23) simplifies to the Exner (1925) equation for conservation of bed material.

Equation (23) requires an additional independent equation for estimating the actual bed-load discharge under non-equilibrium transport conditions. The equation is developed here by applying the conservation equation of sediment mass to a small control volume of the bed-load layer as well as by using the Cheng (1984) approximate expression for the net sediment flux at the layer interface. For a bed level change dominated by the suspended-load and bed-load transports, the resulting equation is expressed as

$$\frac{\partial}{\partial t}\left(\frac{q_b}{U_s}\right) + \frac{\partial q_b}{\partial x} = \frac{q_{bE}-q_b}{L_b}, \tag{24}$$

where U_s is the velocity of the particle in the bed-load zone and can be estimated by the van Rijn (1984a) equation. Equation (24) was previously presented by Wu and Wang (2007). Inserting Equation (22) into Equation (23) results in the following simplified expression for the channel bed evolution:

$$\frac{\partial Z}{\partial t} = \frac{-1}{(1-\lambda_p)}\left(\frac{\Gamma_2\Gamma_3}{3}(kU_\tau c_0) - \overline{w}_s c_0\left(1+(1+\Gamma_1)\Gamma_2\right) + \frac{q_{bE}-q_b}{L_b}\right). \tag{25}$$

It is important to note that the sediment transport model described above solves the transport equations of single-sized, non-cohesive suspended and bed sediments.

2.4. Empirical Equations for Model Closure

The vertically-averaged sediment transport model presented in the preceding section entails an equilibrium bed-load transport equation for model closure. In this study, the sediment load is computed by the Wu et al (2000) empirical equation. The authors' investigation result showed that this empirical equation is more accurate than the van Rijn (1986) equation. It typically requires a pre-determined critical shear stress, which is computed here from the explicit empirical expressions of the curves fitted to the Shields diagram (van Rijn 1984a). Additionally, the recalibrated version of the Komura (1963) formula (Wu and Wang 2006) is used to reckon the initial porosity of

a sediment deposit. The settling velocity of the sediment particle in clear water is estimated by applying the Cheng (1997) formula. Using the initial result, the effective settling velocity of a particle in sediment-laden water is computed by utilizing an equation (Richardson and Zaki 1997) that accounts for the effect of sediment concentration on settling.

3. Numerical Model

3.1. Spatial Discretization and Numerical Flux Computation

Because of the non-linear terms appearing in the governing equations, the solutions of such equations entail a different scheme rather than the classical finite-volume approach for the de Saint-Venant equations. In this study, a standard finite-volume scheme is applied to the conservative form of the equations combined with a finite-difference discretization of the source terms. Such a method is extensively used to solve 1D and 2D higher-order equations (e.g., Soares-Frazão and Guinot 2008, Kim et al 2009). The flow and sediment transport equations can be rewritten in a vector form as follows:

$$\frac{\partial U}{\partial t} + \frac{\partial F(U)}{\partial x} = S, \tag{26}$$

where U, $F(U)$, and S are vectors of the unknown conserved variables, fluxes, and source terms, respectively, and are defined as

$$U = \begin{pmatrix} H \\ q\rho \\ q\rho\left(\beta_4 H_x + Z_x\right) \\ Hc_0\left(1 + \Gamma_1\Gamma_2\right) \\ \dfrac{q_b}{U_s} \\ Z \end{pmatrix}, \tag{27a}$$

$$F(U) = \begin{pmatrix} q \\ \rho\left(\dfrac{q^2}{3H}\beta_1 + \dfrac{gH^2}{2}\right) \\ \dfrac{\rho q^2}{H}\left(\beta_2 H_x + \beta_1 Z_x\right) \\ qc_0 \\ q_b \\ 0 \end{pmatrix}, \tag{27b}$$

$$S = \begin{pmatrix} -\dfrac{1}{\rho}(H\rho_t + q\rho_x) \\ -(\rho g H + p_D)Z_x - \dfrac{\partial}{\partial x}\left(\dfrac{Hp_D}{2}\right) + \dfrac{\partial}{\partial x}(H\overline{\sigma}_x) - \tau_b \\ p_D - \tau_b Z_x + \dfrac{\partial}{\partial x}(H\overline{\tau}_{zx}) + \Psi_2 \\ \dfrac{\Gamma_2\Gamma_3}{3}(kU_\tau c_0) - \overline{w}_s c_0\,(1 + (1+\Gamma_1)\Gamma_2) \\ \dfrac{q_{bE} - q_b}{L_b} \\ \dfrac{-1}{(1-\lambda_p)}\left(\dfrac{\Gamma_2\Gamma_3}{3}(kU_\tau c_0) - \overline{w}_s c_0\,(1 + (1+\Gamma_1)\Gamma_2) + \dfrac{q_{bE} - q_b}{L_b}\right) \end{pmatrix}, \tag{27c}$$

$$\begin{aligned} \Psi_2 = \; & \beta_3 \frac{\partial}{\partial t}(\rho H q_x - qH\rho_x) + \frac{q\rho}{2}q_{xx} + \frac{q^2}{2}\rho_{xx} + \frac{qH}{2}\frac{\partial}{\partial t}(\rho_x) \\ & - q\rho\frac{\partial}{\partial t}(Z_x) - H\rho Z_{tt}. \end{aligned} \tag{27d}$$

For a computational mesh of space-time grid, the finite-volume discretization of the integral form of Equation (26) (Hirsch 2007, p. 208) can be written in the following form using Euler's time stepping method:

$$U_i^{m+1} = U_i^m - \frac{\Delta t}{\Delta x}\left(F(U)_{i+1/2}^m - F(U)_{i-1/2}^m\right) + \Delta t S_i^m, \tag{28}$$

where Δx is the spatial step size in the x-direction, and Δt is the time step. In the above equation, the superscript m denotes the current time level, while $F(U)_{i\pm1/2}$ is the numerical flux exchanged through the boundaries between neighboring cells. Equation (28) is explicitly and implicitly solved at the time levels 1 and 2 to provide additional starting data for the proposed numerical scheme, which will be described in the next section.

The application of the finite-volume method needs reconstructing the conserved variables on the cell interfaces prior to computing the numerical fluxes. In this study, these variables are reconstructed using the fourth-order monotone upstream centered schemes for conservation laws (MUSCL-TVD), which was proposed by Yamamoto and Daiguji (1993). In order to avoid numerical oscillations arising from discontinues bed profile or steep bed gradient, the weighted surface-depth gradient method (Aureli et al 2008) is adopted to determine the flow depth at the cell interfaces. Using the reconstructed interface values, the numerical fluxes are computed by Harten-Lax-van Leer (HLL) approximate Riemann solvers (Harten et al 1983) on a space-time grid, as shown in Fig. 2. Following the method proposed by Toro (2009, pp. 329–331), the required wave speeds are estimated. For the complete solutions of the unknown conserved variables, the computational domain is extended to include ghost cells at the upstream and downstream ends of the actual solution domain (LeVeque 2004, pp. 129–130); their values are extrapolated from interior nodes.

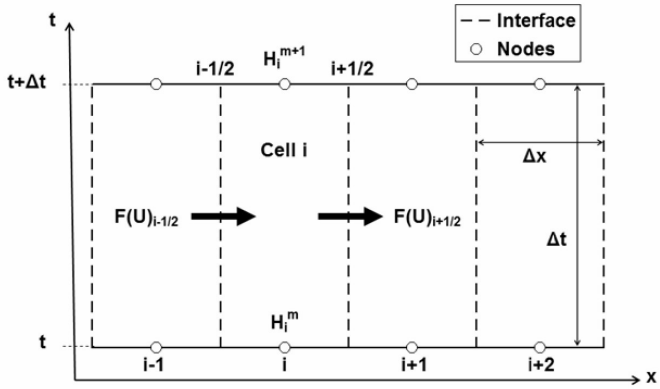

Fig. 2. Computational grid in the $x - t$ plane for a 1D numerical simulation

3.2. Time Integration

Time integration is achieved in two steps using a finite-difference predictor-corrector scheme (Bashforth and Adams 1883). Such a higher-order numerical scheme has been successfully applied to solve complex non-hydrostatic open-channel flow problems (e.g., Wei and Kirby 1995, Kim et al 2009, Zerihun 2021). Using this scheme, the conserved parameters at a time level $m + 1$ are computed from the mixture flow parameters at the time levels m, $m - 1$, and $m - 2$ using explicit and implicit techniques. In the predictor step, the third-order Adams-Bashforth scheme is used to approximate the time derivative term of Equation (26). The resulting discretized equation is

$$U_i^P = U_i^m + \frac{\Delta t}{12}\left(23\Omega_i^m - 16\Omega_i^{m-1} + 5\Omega_i^{m-2}\right), \tag{29a}$$

$$\Omega_i = -\frac{1}{\Delta x}\left(F(U)_{i+1/2} - F(U)_{i-1/2}\right) + S_i, \tag{29b}$$

where the superscript P stands for the predicted cell-averaged values, and i denotes the computational point. In the step of a predictor, Ω_i is determined by using the values of the mixture flow parameters at the known time levels in Equation (29b).

In the corrector step, the time integration is performed by applying the fourth-order Adams-Moulton scheme using the predicted and known cell-averaged values. Equation (26) is discretized by this scheme (Bashforth and Adams 1883), and the resulting expression is given by

$$U_i^C = U_i^m + \frac{\Delta t}{24}\left(9\Omega_i^P + 19\Omega_i^m - 5\Omega_i^{m-1} + \Omega_i^{m-2}\right), \tag{30}$$

where the superscript C refers to the cell-averaged value after the corrector step. For this computational step, the value of Ω_i^P is reckoned from the estimated values of the conserved parameters. The time-varying parameters, appearing in Equation (27d), are

discretized by using the third- and fourth-order accurate finite-difference equations (Bickley 1941) for the predictor and corrector steps, respectively. It is clear that at a time level $m + 1$, the equations of continuity and sediment transport are solved explicitly. However, the solutions of the momentum equations need an implicit technique.

3.3. Implicit Method for the Momentum Equations

For the purposes of accuracy and numerical stability, Equations (11) and (12) are solved implicitly for the unknown conserved variables q and p_D at both the predictor and corrector steps. A similar approach was successfully applied to solve complex open-channel flow problems (e.g., Erduran et al 2005, Soares-Frazão and Guinot 2008). Using the finite-difference approximations for the source terms, the discretized forms of these momentum equations for the predictor step can be written as

$$q_i^P \rho_i^P + \frac{23\Delta t}{12}\left(p_{D,i}^m\left(\frac{Z_{i+1}^m - Z_{i-1}^m}{2\Delta x}\right) + \left(\frac{H_{i+1}^m p_{D,i+1}^m - H_{i-1}^m p_{D,i-1}^m}{4\Delta x}\right)\right) - q_i^m \rho_i^m - \frac{23\Delta t}{12}\Psi_{1,i}^m - \frac{\Delta t}{12}\left(-16\Omega_i^{m-1} + 5\Omega_i^{m-2}\right) = 0, \tag{31a}$$

$$\Psi_{1,i}^m = -\frac{1}{\Delta x}\left(\left(\rho\left[\frac{q^2}{3H}\beta_1 + \frac{gH^2}{2}\right]\right)_{i+1/2}^m - \left(\rho\left[\frac{q^2}{3H}\beta_1 + \frac{gH^2}{2}\right]\right)_{i-1/2}^m\right) - g\rho_i^m H_i^m\left(\frac{Z_{i+1}^m - Z_{i-1}^m}{2\Delta x}\right) + \left(\frac{H_{i+1}^m \overline{\sigma}_{x,i+1}^m - H_{i-1}^m \overline{\sigma}_{x,i-1}^m}{2\Delta x}\right) - \tau_{b,i}^m, \tag{31b}$$

$$q_i^P \rho_i^P\left(\beta_4\left(\frac{H_{i+1}^P - H_{i-1}^P}{2\Delta x}\right) + \left(\frac{Z_{i+1}^P - Z_{i-1}^P}{2\Delta x}\right)\right) - \frac{23\Delta t}{12} p_{D,i}^m - q_i^m \rho_i^m\left(\beta_4\left(\frac{H_{i+1}^m - H_{i-1}^m}{2\Delta x}\right) + \left(\frac{Z_{i+1}^m - Z_{i-1}^m}{2\Delta x}\right)\right) - \frac{23\Delta t}{12}\Psi_{3,i}^m - \frac{\Delta t}{12}\left(-16\Omega_i^{m-1} + 5\Omega_i^{m-2}\right) = 0, \tag{32a}$$

$$\Psi_{3,i}^m = -\frac{1}{\Delta x}\left(\left(\frac{\rho q^2}{H}\left[\beta_2 H_x + \beta_1 Z_x\right]\right)_{i+1/2}^m - \left(\frac{\rho q^2}{H}\left[\beta_2 H_x + \beta_1 Z_x\right]\right)_{i-1/2}^m\right) + \left(\frac{H_{i+1}^m \overline{\tau}_{zx,i+1}^m - H_{i-1}^m \overline{\tau}_{zx,i-1}^m}{2\Delta x}\right) - \tau_{b,i}^m + \Psi_{2,i}^m. \tag{32b}$$

Using a similar technique as above, the implicit forms of the discretized momentum equations for the corrector step become

$$q_i^C \rho_i^C + \frac{9\Delta t}{24}\left(p_{D,i}^m\left(\frac{Z_{i+1}^P - Z_{i-1}^P}{2\Delta x}\right) + \left(\frac{H_{i+1}^P p_{D,i+1}^m - H_{i-1}^P p_{D,i-1}^m}{4\Delta x}\right)\right) - q_i^m \rho_i^m - \frac{9\Delta t}{24}\Psi_{1,i}^P - \frac{\Delta t}{24}\left(19\Omega_i^m - 5\Omega_i^{m-1} + \Omega_i^{m-2}\right) = 0, \tag{33}$$

$$
\begin{aligned}
&q_i^C \rho_i^C \left(\beta_4 \left(\frac{H_{i+1}^C - H_{i-1}^C}{2\Delta x} \right) + \left(\frac{Z_{i+1}^C - Z_{i-1}^C}{2\Delta x} \right) \right) - \frac{9\Delta t}{24} p_{D,i}^m \\
&- q_i^m \rho_i^m \left(\beta_4 \left(\frac{H_{i+1}^m - H_{i-1}^m}{2\Delta x} \right) + \left(\frac{Z_{i+1}^m - Z_{i-1}^m}{2\Delta x} \right) \right) - \frac{9\Delta t}{24} \Psi_{3,i}^P \\
&- \frac{\Delta t}{24} \left(19\Omega_i^m - 5\Omega_i^{m-1} + \Omega_i^{m-2} \right) = 0.
\end{aligned} \tag{34}
$$

In the above equations, all of the fluxes and source terms are evaluated using the known variable values at the previous time levels. This leads to a system of non-linear equations that requires a numerical linearization procedure. Equations (31)–(34) may be written in the following general form:

$$
\Phi_{1,i} q_i^{m+1} + \Phi_{2,i+1} p_{D,i+1}^m + \Phi_{3,i} p_{D,i}^m + \Phi_{4,i-1} p_{D,i-1}^m = \Phi_5, \tag{35}
$$

where $\Phi_1, \Phi_2, \ldots, \Phi_5$ are coefficients, which can be determined by comparing Equation (35) with the corresponding discretized equations. The resulting implicit set of non-linear equations is first linearized by the Newton-Raphson method and then solved by means of the lower-upper (LU) decomposition method, as was done by Zerihun (2016, 2019).

4. Numerical Tests and Results

The applicability of the proposed model is examined by considering different types of sediment-laden, quasi-hydrostatic and non-hydrostatic flow problems. The selected problems have different characteristics and require different techniques to simulate them accurately. The inflow and outflow sections of their computational domains are located in the hydrostatic flow region, where no or negligible morphological changes are expected to occur. For all test cases, the flow depth, discharge, and the mean sediment concentrations of the suspended load and bed load were specified as boundary conditions at the upstream end section. Besides, these boundary values were specified at the interior nodes as initial values ($t = 0$ s) to commence the iteration process for test cases with a wet-bed condition throughout the computational domain. For cases with a combination of wet and dry beds, a flow depth of 1 mm was specified as an initial value in the dry-bed zone to avoid undesirable numerical instability arising from infinite values of the fluxes due to a nil value of the conserved variable.

For selected parameters, a sensitivity analysis was performed prior to the tasks of model verification. The results demonstrate that the numerical solutions are the least sensitive to the non-equilibrium adaptation length of bed-load transport (L_b) and the empirical coefficients Γ_3 and μ, but more sensitive to the coefficient of roughness and spatial step size. Hence, the spatial step size was varied from 7.5 to 500 mm, depending on the nature of the flow problems. For the quasi-uniform flow cases, a coarser step size was used without any stability and accuracy issues. Additionally, the computational time step is limited by a numerical stability criterion such as the

Courant-Friedrichs-Lewy (CFL) condition. A CFL value between 0.1 and 0.45 was employed to obtain stable and reliable results. Therefore, the numerical results presented hereafter are independent of the sizes of the computational steps.

4.1. Test Case 1: Suspended Sediment Discharge in Prismatic Channels

A large set of available experimental data (Guy et al 1966, Montes 1973) was used to calibrate and verify the results of the model. These experiments were conducted in the laboratory flumes to study the hydraulic characteristics of the fluid-sediment mixture for a wide range of flow conditions. The velocity profiles and the suspended sediment concentration at the downstream end section were measured. Fig. 3a shows the vertical profile of the horizontal velocity. In the suspended-load layer, the computed non-dimensional horizontal velocity profile, $\vartheta (= u/\overline{U}$, where $\overline{U}$ is the depth-averaged horizontal velocity), showed a fairly good correlation with the measured data, with a correlation coefficient of 0.8. Near the channel bed ($\Lambda < 0.1$), the predicted velocity profile appreciably deviated from the measured data. The measured velocity data reported by Guy et al (1966) might have some irregularities due to the effects of flow turbulence. Since an empirical equation is used to estimate the bed load, this deviation does not significantly affect the quality of the model results.

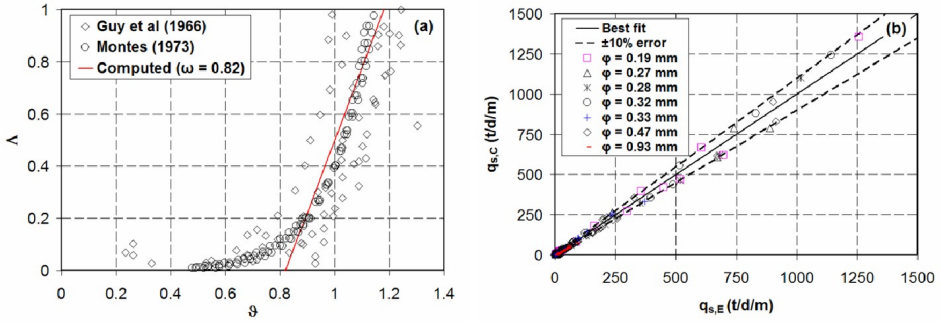

Fig. 3. (a) Horizontal velocity distribution; and (b) comparison of the computed result, $q_{s,C}$, with the measured suspended sediment discharge, $q_{s,E}$ (data from Guy et al (1966)). The mean sediment diameter is indicated by φ

Figure 3b shows the comparison of the simulated suspended sediment discharge at the downstream end with the experimental data reported by Guy et al (1966). The selected data include the average sediment discharges from the experiments conducted in sand bed flumes for flow between 44 and 643 L/s. These data were collected in a recirculating flume 2.44 m wide, 610 mm deep, and 45.72 m long. The mean sediment diameter of the sand varied from 0.19 to 0.93 mm. As shown in the figure, most of the computed results fell within the region of ±10%. Only 15% of the computed values deviated from the measured sediment discharges by more than 10%.

4.2. Test Case 2: Sediment Transport in a Dredged Trench

The migration of dredged trenches with different side slopes were experimentally studied by the Delft Hydraulics Laboratory [DHL] (1980). The experiments, which were conducted in trenches with initial side slopes 5.7 and 18.4° and inflow discharge 200 L/s/m (Tests T1 and T3), were selected for verifying the numerical results. These experiments were carried out in a laboratory flume with a bed made of fine sand (median diameter φ_{50} = 0.16 mm). The flume was 500 mm wide, 700 mm deep, and 30 m long. Sand with similar characteristics to the bed material was supplied at a total loading rate of 0.04 kg/s/m at the upstream end section for maintaining equilibrium conditions at this section. The bed level changes due to deposition and erosion were measured at different times by means of an automatic sounding system.

The computed bed profiles at 7.5 and 15 h are presented in Fig. 4. In this figure, the variation of the normalized bed elevation, $Z_N (= Z/H_0$, where H_0 is the flow depth at the inflow section), with the normalized horizontal distance, $X (= x/H_0)$, is shown. For both cases, the numerical model satisfactorily mimics the deposition and erosion processes in the trench. In the acceleration zone ($13 \leq X < 19$), however, some minor discrepancy between the computed and measured erosion levels can be seen at a computational time of 15 h. In general, the elevations of the bed profiles are predicted reasonably well with a mean absolute relative error of 8.4%.

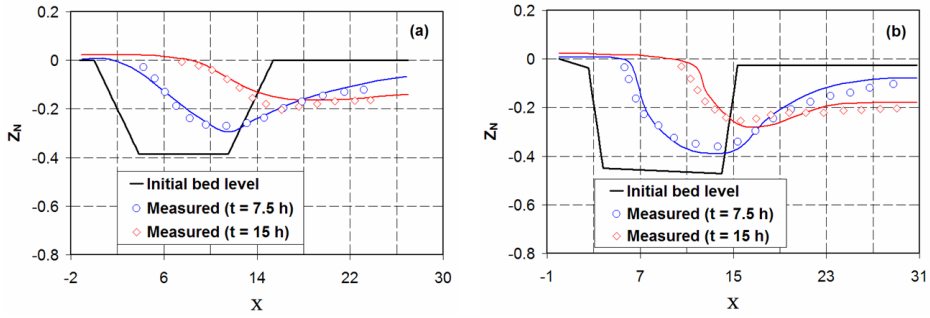

Fig. 4. Bed profiles due to siltation and erosion of dredged trenches with different initial side slopes: (a) Test T3 (side slope = 5.7°); and (b) Test T1 (side slope = 18.4°). The computed results are shown in solid lines with the colors of the corresponding experimental data (DHL 1980)

4.3. Test Case 3: Subcritical Flow over a Stepped Channel Bed

Tingsanchali and Supharatid (1996) conducted a series of experiments on subcritical flows over a movable flume bed made of a nearly uniform sand (φ_{50} = 0.90 mm). The flume had a width of 600 mm and a test section with a length of 12 m. A test run with a constant inflow discharge of 54 L/s and no initial sediment loading was selected to

validate the results of the model. For this run, the initial bed profile had a uniform thickness of 200 mm for a length of 6 m. This thickness was gradually reduced to 100 mm at the rate of 10% and then remained constant. The free-surface and bed elevations along the centerline of the flume were measured using an automatic profile recorder.

Figure 5 compares the normalized free-surface elevation, $\eta_N (= \eta/H_0)$, and bed level with the experimental data. As can be seen, the numerical model accurately predicted the free-surface profile. For this subcritical flow situation, the effect of the streamline curvature is insignificant, except in the flow region near the stepped-bed of the channel. Upstream of the initial slanted face of the bed ($X \leq 35$), the elevation of the modified bed profile due to erosion was slightly overestimated by the model. In the deposition region, the computed bed level agreed reasonably well with the experimental data.

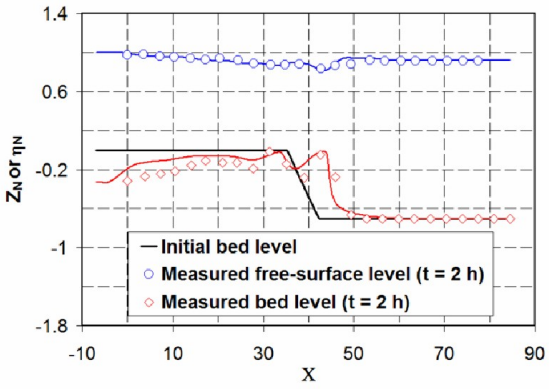

Fig. 5. Comparison of the results of the model with the measured data for free-surface and bed profiles. The computed results are shown in solid lines with the colors of the corresponding experimental data

4.4. Test Case 4: Dike Erosion due to an Overtopping Flow

4.4.1. Schmocker's (2011) Experiment

A series of experiments on dike erosion due to an overtopping flow was carried out by Schmocker (2011). These experiments were performed in a straight rectangular 8 m long, 400 mm wide, and 700 mm deep flume. The results of Test 52, which was conducted using a trapezoidal-shaped dike made of coarse sand with a mean sediment size of 2 mm, were selected to validate the model results. The dike had a crest length of 100 mm and a symmetrical face slope of 26.57°. During the experiment, a constant inflow discharge of 8 L/s was sustained. The seepage through the dike was controlled

by providing upstream drainage underneath the dike. The free-surface and bed profiles at various times were recorded using a 30 Hz CCD camera.

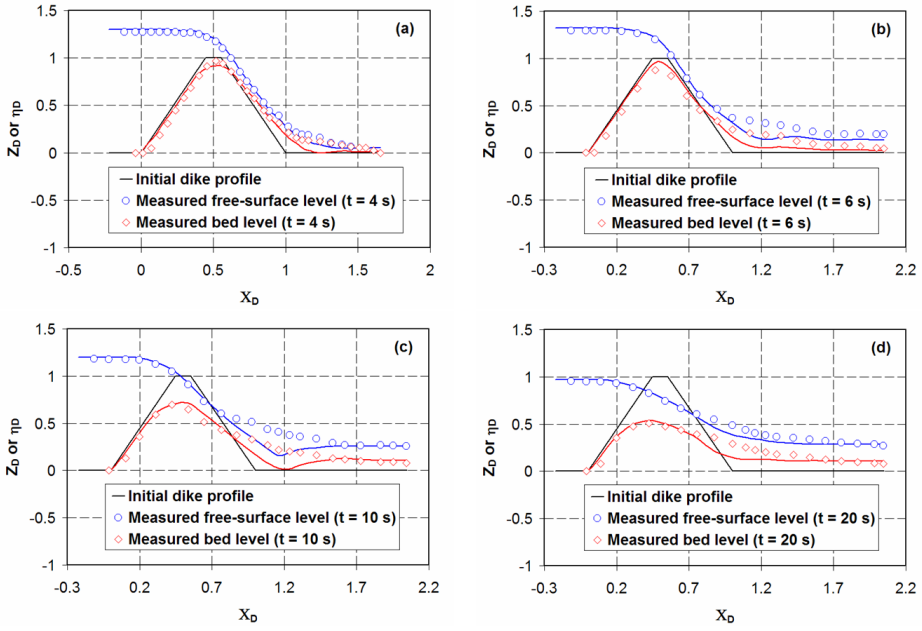

Fig. 6. Temporal change in free-surface and bed elevations for a dike with upstream bottom drainage. The computed results are shown in solid lines with the colors of the corresponding experimental data of Schmocker (2011)

Figure 6 shows the non-dimensional elevations of the free surface, $\eta_D (= \eta/H_D$, where H_D is the initial height of the dike), and bed, $Z_D (= Z/H_D)$, as a function of $X_D (= x/L_D$, where L_D is the initial bottom length of the dike) for various dike breaching phases. The starting time of the overtopping process ($t = 0$ s) was the time when the level of the free surface in the reservoir reached the upstream edge of the crest. As depicted in the figure, the processes of plane dike breaching at various times were satisfactorily simulated by the model. However, the volume of the transported and deposited material near the toe of the dike was not accurately predicted. As a result, the elevations of the free surface and the bed were underestimated in the downstream flow region. This discrepancy is attributed to the effect of pore-water pressure, which was not successfully reduced by the bottom drainage especially at the later stage of the breaching process (Liang et al 2020). It is obvious that high pore-water pressure triggers instability of the downstream-face slope (Pickert et al 2011) and hence sliding of the dike body. Such complex processes cannot be handled by the proposed numerical model.

4.4.2. Tabrizi's (2016) Experiment

The results of the model were also compared with the experimental data of Tabrizi (2016). Similar to Schmocker (2011), he conducted experiments to examine the surface erosion process of a trapezoidal-shaped dike, which was built of non-compacted, uniform sand material with a mean diameter of 0.55 mm. This 150 mm high dike had upstream- and downstream-face slopes of 26.57° and was tested in a rectangular flume 200 mm wide, 250 mm deep, and 6.1 m long for a constant inflow discharge of 0.5 L/s. The seepage through the dike was controlled by placing a thin clay layer on its upstream face (see Fig. 7a). The free-surface and bed profiles at various times were recorded using a high definition video camera.

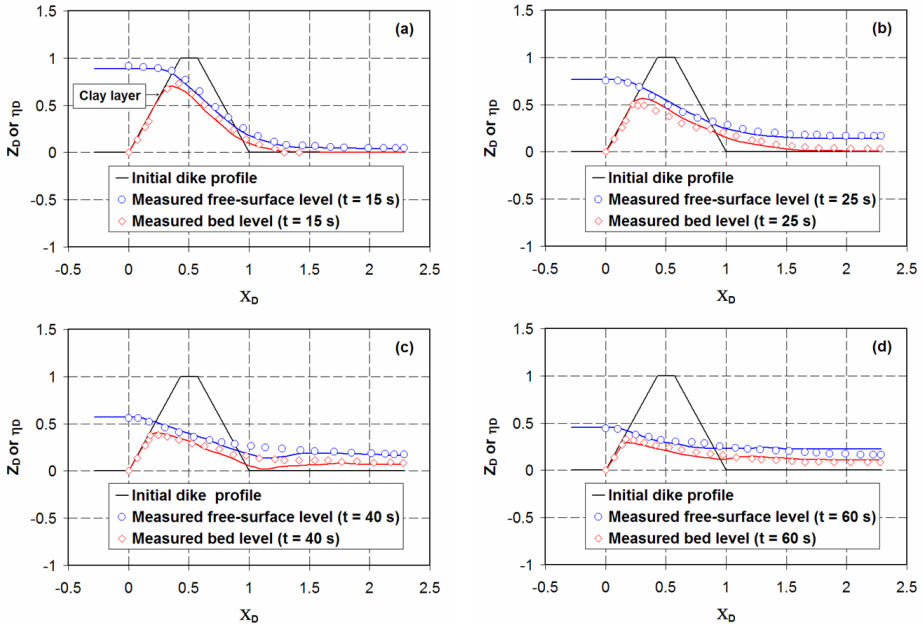

Fig. 7. Temporal change in free-surface and bed elevations for a dike with upstream bottom drainage. The computed results are shown in solid lines with the colors of the corresponding experimental data of Schmocker (2011)

Figure 7 shows a comparison between the measured and the computed temporal change in free-surface and bed elevations. In the upstream flow region ($X_D < 0.7$), the model adequately predicted the levels of the free surface and bed at all stages of breaching. Similar to the previous test, however, it underestimated the levels of the deposited material in the vicinity of the dike toe, as shown in Fig. 7b,c. At the later stages of breaching, the predicted levels of deposition fairly agreed with the measurements. During these stages, the dike slopes were rapidly flattened (see Figs. 6d and

7c,d). Consequently, the effect of non-hydrostatic pressure became almost insignificant. Only for the case of curvilinear transcritical overflows, such a dynamic pressure effect can play a dominant role (Zerihun and Fenton 2007, Zerihun 2020). Considering the complicated aspects of the dike erosion problem, the overall characteristics of the 2D dike breaching were reasonably reproduced.

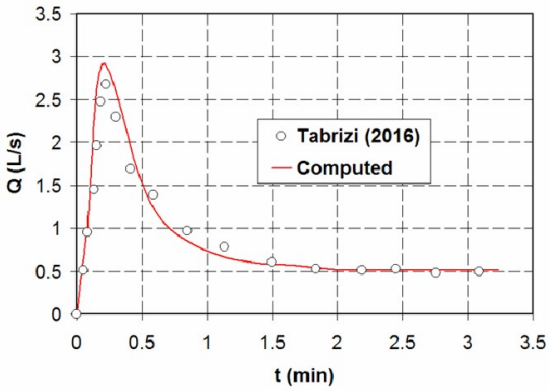

Fig. 8. An outflow hydrograph corresponding to a 2D breaching of a dike

The variation of the outflow discharge over time is depicted in Fig. 8. The general trend of the temporal change of the outflow discharge was accurately portrayed by the model. It can be seen from this figure that at the later stages of breaching, the flow approached a quasi-steady flow condition. The peak discharge and the time to peak were predicted with errors of 8.7 and 9.3%, respectively. The results of both tests confirmed that in the region, where the flow regime changes from a sub- to a super-critical state, the model satisfactorily simulates the process of plane dike erosion irrespective of the degree of the streamline curvatures. As was the case for a shallow-water modeling approach (see, e.g., Mizutani et al 2013), its performance in the supercritical flow region immediately downstream of the dike toe can be improved by accounting for the effects of sub-surface flow, thereby simultaneously solving the problems of erosion and infiltration.

4.5. Test Case 5: Dam-Break Flow over a Movable Bed

The performance of the numerical model was further evaluated by simulating a dam-break flow over a movable bed. The laboratory experiment of Fraccarollo and Capart (2002) was selected to validate the numerical results. They performed the experiment in a horizontal prismatic flume of 100 mm wide, 350 mm deep, and 2.5 m long. The flume bed was covered by light cylindrical polyvinyl chloride (PVC) pellets with an equivalent spherical diameter of 3.5 mm and a specific gravity of 1.54. The idealized dam was represented by a vertical sluice gate, which was lowered down to the flume

bed (see Fig. 9a). The initial water depth in the upstream reservoir was 100 mm, and the test section downstream of the gate was initially dry. The dam-break flow at various times was recorded using a fast CCD camera, operating at the rate of 200 frames per second.

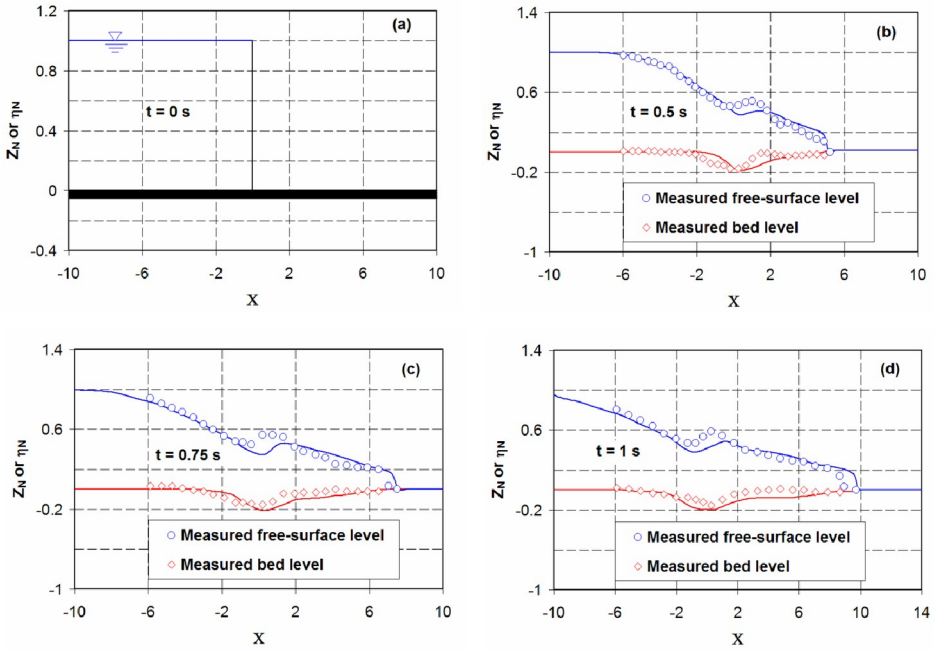

Fig. 9. (a) Schematic diagram of the initial stage of the dam break. In (b), (c) and (d), the simulated free-surface and bed profiles at various dam-break stages are compared with the measured data. The computed results are shown in solid lines with the colors of the corresponding experimental data of Fraccarollo and Capart (2002)

The simulated free-surface and bed profiles at various dam-break stages are shown in Fig. 9b–d. The predictions of the model for the scour pattern and partial re-deposition of bed material were fairly agreed with the measurements. In the flow region behind the wavefront ($X \geq 0$), the model slightly underestimated the bed levels. Upstream of this region, the bed level was overestimated at the earlier dam-break time of 0.5 s. As can be seen, the trend of the dam-break wave was fairly simulated by the model, including the location of the wavefront. Upstream and downstream of the scour hole, the elevations of the free surface were predicted reasonably well by the model. In the flow region around the scour hole, however, the free-surface elevation of the hydraulic jump was underestimated. The main reasons for the discrepancy between the results of the model and the experimental data are the 3D characteristics of the hydraulic jump near the initial gate site and the debris flow behavior (see,

e.g., Suwa 1988, Takahashi 2014, pp. 29–31) of the highly concentrated mixture flow near the wavefront. Such complex characteristics of the fluid-granular flow cannot be accurately simulated by the proposed model. Overall, the effect of the vertical acceleration on the characteristics of the dam-break flow was successfully accounted for by the model's higher-order Boussinesq-type correction.

5. Summary and Conclusions

In this study, a higher-order numerical model for analyzing the problems of non-cohesive sediment transport in open channels was proposed. The governing equations of the model encompass the depth-averaged Boussinesq-type equations for hydrodynamics, an Exner-type equation for morphodynamics, one-dimensional transport equations for the suspended and bed sediments, and a set of empirical equations for an equilibrium bed-load transport and estimations of the various parameters. A hybrid finite-volume and finite-difference scheme was employed to discretize and solve the non-linear governing equations. The ability of the model to successfully predict the temporal variations of the bed elevation and sediment transport rate was examined by considering quasi-hydrostatic and non-hydrostatic open-channel flows over movable beds, and its results were compared with the experimental data available.

The following conclusions are drawn from this study:

1. For the case of migration of dredged trenches, the numerical model satisfactorily portrayed the deposition and erosion processes with a minor discrepancy between the computed and measured erosion levels in the acceleration zone ($13 \leq X < 19$). A comparable model performance result was also obtained for the test case of subcritical flow over a movable stepped channel bed. The overall results attested the capability of the model for simulating the salient features of a sediment-laden, weakly non-hydrostatic open-channel flow.
2. The proposed model was also tested for a sediment transport situation in open channels where bed load is more important such as plane dike erosion. The results of the tests reveal that the model can adequately simulate the outflow discharge and the process of dike erosion. However, the sliding of the dike body caused by the sub-surface flow affects the quality of the model results, especially in the supercritical flow region immediately downstream of the dike toe. To improve the performance of the current model, the effects of sub-surface flow on dike breaching must be accounted for by coupling this model with a seepage flow and slope stability models. This issue will be addressed in depth in a subsequent publication.
3. For the dam-break flow, the trend of the dam-break wave was fairly simulated by the model, including the location of the wavefront. In spite of the 3D characteristics of the flow, the elevations of the free surface in the flow regions upstream and downstream of the scour hole were predicted reasonably well by the model. Furthermore, the undular characteristics of the free-surface profile were success-

fully reproduced, demonstrating the model's capability for handling the effect of the vertical acceleration on dam-break flow.

The results of this investigation reveal that the proposed model is a promising morphodynamic tool for analyzing real-life problems related to flow-induced sediment transport processes in open channels. Its results may be applied to develop a risk assessment and management strategy for a riverine infrastructure.

References

Aureli F., Maranzoni A., Mignosa P., Ziveri C. (2008) A weighted surface-depth gradient method for the numerical integration of the 2D shallow-water equations with topography, *Adv. Water Resour.*, **31**(7), 962–974.

Bashforth F., Adams J. C. (1883) *An Attempt to Test the Theories of Capillary Action by Comparing the Theoretical and Measured Forms of Drops of Fluid, with an Explanation of the Method of Integration Employed in Constructing the Tables which Give the Theoretical Forms of Such Drops*, Cambridge University Press, Cambridge, UK, 18–19.

Bechteler W., Schrimpf W. (1984) Improved numerical model for sedimentation, *J. Hydraul. Eng.*, **110**(3), 234–246.

Bechteler W., Schrimpf W. (1988) Practical aspects for the application of the diffusion-convection theory for sediment transport in turbulent flows, [In:] *Developments in Water Science*, Celia et al (eds.), Elsevier, **35**, 351–356, doi:10.1016/S0167-5648(08)70360-5.

Bennett J. P. (1974) Concepts of mathematical modeling of sediment yield, *Water Resour. Res.*, **10**(3), 485–492.

Berger R. C. (1992) *Free-surface Flow over Curved Surfaces*, Ph.D. Thesis, University of Texas, Austin, TX, USA.

Bickley W. G. (1941) Formulae for numerical differentiation, *Math. Gaz.*, **25**(263), 19–27, doi:10.2307/3606475.

Boussinesq J. (1877) *Essai Sur la Théorie des Eaux Courantes* [*Essay on the Theory of Water Flow*], Mémoires Présentés par Divers Savants à l'Académie des Sciences, Paris, **23**(1), 1–680 [in French].

Cantero-Chinchilla F. N., Castro-Orgaz O., Khan A. A. (2019) Vertically averaged and moment equations for flow and sediment transport, *Adv. Water Resour.*, doi:10.1016/j.advwatres.2019.103387.

Cao Z., Pender G., Wallis S., Carling P. (2004) Computational dam-break hydraulics over erodible sediment bed, *J. Hydraul. Eng.*, **130**(7), 689–703.

Capart H., Young D. L. (1998) Formation of a jump by the dam-break wave over a granular bed, *J. Fluid Mech.*, **372**, 165–187.

Cheng K. J. (1984) Bottom-boundary condition for non-equilibrium transport of sediment, *J. Geophys. Res.*, **89**(C5), 8209–8214.

Cheng N. S. (1997) Simplified settling velocity formula for sediment particle, *J. Hydraul. Eng.*, **123**(2), 149–152.

Daubert A., Lebreton J. C. (1967) Etude expérimentale sur modèle mathématique de quelques aspects des processus d'érosion des lits alluvionnaires, en régime permanent et nonpermanent [Experimental study on a mathematical model of some aspects of the erosion processes of alluvial beds, in steady and unsteady states], [In:] *Proceedings of the 12th IAHR World Congress*, Fort Collins, CO, USA, 11–14 Sept., 3, 26–37 [in French].

Delft Hydraulics Laboratory (1980) *Storm Surge Barrier Oosterschelde, Computation of Siltation in Dredged Trenches: Mathematical Model*, Report 1267-V/M 1570, Delft, The Netherlands.

Elgamal M. H., Steffler P. M. (2001) Stability analysis of dunes using 1D depth-averaged flow models, [In:] *Proceedings of the 2nd IAHR Symposium on Rivers, Coastal and Estuarine Morphodynamics*, Obihiro, Japan, 10–14 Sept., 197–206.

El Kadi Abderrezzak K., Paquier A. (2009) One-dimensional numerical modeling of sediment transport and bed deformation in open channels, *Water Resour. Res.*, **45**, W05404, doi:10.1029/2008WR007134.

Erduran K. S., Ilic S., Kutija V. (2005) Hybrid finite-volume finite-difference scheme for the solution of Boussinesq equations, *Int. J. Numer. Meth. Fluids*, **49**, 1213–1232.

Exner F. M. (1925) *Über die Wechselwirkung Zwischen Wasser und Geschiebe in Flüssen* [*On the Interaction between Water and Debris in Rivers*], Sitzungsberichte der Akademie der Wissenschaften mathematisch-naturwissenschaftliche Klasse, **134**(2a), 165–203 [in German].

Ferziger J. H., Peric M. (2002) *Computational Methods for Fluid Dynamics*, 3rd rev. ed., Springer-Verlag Berlin Heidelberg: New York, NY, USA.

Fischer B. H., List E. J., Koh R. C., Imberger J., Brooks N. H. (1979) *Mixing in Inland and Coastal Waters*, Academic Press: New York, NY, USA.

Fraccarollo L., Capart H. (2002) Riemann wave description of erosional dam-break flows, *J. Fluid Mech.*, **461**, 183–228.

Franzini F., Soares-Frazão S. (2018) Coupled finite-volume scheme with adapted Augmented Roe scheme for simulating morphological evolution in arbitrary cross-sections, *J. Hydroinformatics*, **20**, 1111–1130.

Ghamry H. K. (1999) *Two-Dimensional Vertically Averaged and Moment Equations for Shallow Free-Surface Flows*, Ph.D. Thesis, University of Alberta, Edmonton, AB, Canada.

Guo Q. C., Jin Y. C. (1999) Modeling sediment transport using depth-averaged and moment equations, *J. Hydraul. Eng.*, **125**(12), 1262–1269.

Guy H. P., Simons D. B., Richardson E. V. (1966) *Summary of Alluvial Channel Data from Flume Experiments*, 1956–61, Professional Paper 462-I, USGS, Washington, DC, USA.

Harten A., Lax P. D., van Leer B. (1983) On upstream differencing and Godunov-type scheme for hyperbolic conservation laws, *SIAM Rev. Soc. Ind. Appl. Math.*, **25**(1), 35–61.

Hirsch C. (2007) *Numerical Computation of Internal and External Flows: Vol. 1 Fundamentals of Computational Fluid Dynamics*, 2nd ed., Elsevier: Oxford, UK.

Jin Y., Li B. (1996) The use of a one-dimensional depth-averaged moment of momentum equation for the non-hydrostatic pressure condition, *Can. J. Civ. Eng.*, **23**, 150–156.

Karim F. (1995) Bed configuration and hydraulic resistance in alluvial-channel flows, *J. Hydraul. Eng.*, **121**(1), 15–25.

Kim D. H., Lynett P. J., Socolofsky S. (2009) A depth-integrated model for weakly dispersive, turbulent, and rotational fluid flows, *Ocean Model.*, **27**(3–4), 198–214.

Komura S. (1963) Discussion of "Sediment Transportation Mechanics: Introduction and Properties of Sediment, Progress Report by the Task Committee on Preparation of Sedimentation Manual of the Committee on Sedimentation of the Hydraulics Division", *J. Hydraul. Div.*, **89**(HY1), 263–266. doi:10.1061/JYCEAJ.0000837.

LeVeque R. J. (2004) *Finite-Volume Methods for Hyperbolic Problems*, Cambridge University Press: Cambridge, UK.

Liang D., Zhao X., Soga K. (2020) Simulation of overtopping and seepage induced dike failure using two-point MPM, *Soils Found.*, **60**, 978–988.

Lin B. N. (1984) Current study of unsteady transport of sediment in China, [In:] *Proceedings of the Japan–China Bilateral Seminar on River Hydraulics and Engineering Experiences*, Tokyo, Kyoto, and Sapporo, Japan, 23 July–6 Aug., 337–342.

Marsooli R., Wu W. (2015) Three-dimensional numerical modeling of dam-break flows with sediment transport over movable beds, *J. Hydraul. Eng.*, **141**, doi:10.1061/(ASCE)HY.1943-7900.0000947.

Mizutani H., Nakagawa H., Yoden T., Kawaike K., Zhang H. (2013) Numerical modeling of river embankment failure due to overtopping flow considering infiltration effects, *J. Hydraul. Res.*, **51**(6), 681–695.

Montes J. S. (1973) *Interaction of Two-Dimensional Turbulent Flow with Suspended Particles*, Ph.D. Thesis, Massachusetts Institute of Technology, Boston, MA, USA.

Pickert G., Weitbrecht V., Bieberstein A. (2011) Breaching of overtopped river embankments controlled by apparent cohesion, *J. Hydraul. Res.*, **49**(2), 143–156.

Pontillo M., Schmocker L., Greco M., Hager W. H. (2010) One-dimensional numerical evaluation of dike erosion due to overtopping, *J. Hydraul. Res.*, **48**(5), 573–582.

Ramirez-León H., Cuevas C. R., Díaz E. H. (2005) Multilayer hydrodynamic models and their application to sediment transport in estuaries, [In:] *Current Trends in High Performance Computing and Its Applications*, Zhang et al (eds.), Springer, 59–70, doi:10.1007/3-540-27912-1_6.

Reynolds O. (1895) On the dynamical theory of incompressible viscous fluids and the determination of the criterion, *Philos. Trans. Royal Soc. A*, **186**, 123–164, doi:10.1098/rsta.1895.0004.

Richardson J. F., Zaki W. N. (1997) Sedimentation and fluidization: Part I, *Chem. Eng. Res. Des.*, **75**(1), S82–S100. doi:10.1016/S0263-8762(97)80006-8.

Rowan T. (2019) *Advances in Modeling and Numerical Simulation of Sediment Transport in Shallow-Water Flows*, Ph.D. Thesis, Durham University, Durham, UK.

Schlichting H., Gersten K. (2017) *Boundary-Layer Theory*, 9th ed., Springer-Verlag GmbH Berlin Heidelberg, Germany.

Schmocker L. (2011) *Hydraulics of Dike Breaching*, Ph.D. Thesis, Swiss Federal Institute of Technology (ETH), Zürich, Switzerland.

Soares-Frazão S., Guinot V. (2008) A second-order semi-implicit hybrid scheme for one-dimensional Boussinesq-type waves in rectangular channels, *Int. J. Numer. Methods Fluids*, **58**(3), 237–261.

Steffler P. M., Jin Y. (1993) Depth averaged and moment equations for moderately shallow free-surface flow, *J. Hydraul. Res.*, **31**(1), 5–17.

Suwa H. (1988) *Focusing Mechanisms of Large Boulders to a Debris-Flow Front*, Disaster Prevention Research Institute, Kyoto University, Kyoto, Japan.

Tabrizi A. A. (2016) *Modeling Embankment Breach due to Overtopping*, Ph.D. Thesis, University of South Carolina, Columbia, SC, USA.

Takahashi T. (2014) *Debris Flow: Mechanics, Prediction and Counter Measures*, 2nd ed. CRC Press, Taylor and Francis Group: Boca Raton, FL, USA.

Tingsanchali T., Supharatid S. (1996) Experimental investigation and analysis of HEC-6 river morphological model, *Hydrol. Process.*, **10**, 747–761.

Toro E. F. (2009) *Riemann Solvers and Numerical Methods for Fluid Dynamics: A Practical Introduction*, 3rd ed., Springer-Verlag Berlin Heidelberg, Germany.

van Rijn L. C. (1984a) Sediment transport, Part I: Bed-load transport, *J. Hydraul. Eng.*, **110**(10), 1431–1456.

van Rijn L. C. (1984b) Sediment transport, Part II: Suspended-load transport, *J. Hydraul. Eng.*, **110**(11), 1613–1641.

van Rijn L. C. (1986) Mathematical modeling of suspended sediment in non-uniform flows, *J. Hydraul. Eng.*, **112**(6), 433–455.

Vasquez J. A., Millar R. G., Steffler P. M. (2011) Vertically averaged and moment model for meandering river morphology, *Can. J. Civ. Eng.*, **38**(8), 921–931.

Vreugdenhil C. B. (1994) *Numerical Methods for Shallow-Water Flow*, Kluwer Academic Publishers: Dordrecht, The Netherlands.

Wai O., Lu Q., Li Y. S. (1996) Multilayer modeling of three-dimensional hydrodynamic transport processes, *J. Hydraul. Res.*, **34**(5), 677–693.

Wei G., Kirby J. T. (1995) Time-dependent numerical code for extended Boussinesq equations, *J. Waterw. Port Coast. Ocean Eng.*, **121**(5), 251–261.

Wu W., Wang S. S. Y., Jia Y. (2000) Non-uniform sediment transport in alluvial rivers, *J. Hydraul. Res.*, **38**(6), 427–434.

Wu W., Wang S. S. Y. (2006) Formulas for sediment porosity and settling velocity, *J. Hydraul. Eng.*, **132**(8), 858–862.

Wu W., Wang S. S. Y. (2007) One-dimensional modeling of dam-break flow over movable beds, *J. Hydraul. Eng.*, **133**(1), 48–58.

Wu W., Wang S. S. Y. (2008) One-dimensional explicit finite-volume model for sediment transport, *J. Hydraul. Res.*, **46**(1), 87–98.

Xia J., Lin B., Falconer A. R., Wang G. (2010) Modeling dam-break flows over mobile beds using a 2D coupled approach, *Adv. Water Resour.*, **33**(2), 171–183.

Yamamoto S., Daiguji H. (1993) Higher-order accurate upwind schemes for solving the compressible Euler and Navier-Stokes equations, *Comput. Fluids*, **22**(2–3), 259–270.

Zerihun Y. T. (2004) *A One-Dimensional Boussinesq-Type Momentum Model for Steady Rapidly-Varied Open-Channel Flows*, Ph.D. Thesis, The University of Melbourne, Melbourne, Vic, Australia.

Zerihun Y. T., Fenton J. D. (2006) One-dimensional simulation model for steady transcritical free-surface flows at short length transitions, *Adv. Water Resour.*, **29**(11), 1598–1607.

Zerihun Y. T., Fenton J. D. (2007) A Boussinesq-type model for flow over trapezoidal profile weirs, *J. Hydraul. Res.*, **45**(4), 519–528.

Zerihun Y. T. (2016) Modeling free-surface flow with curvilinear streamlines by a non-hydrostatic model, *J. Hydrol. Hydromech.*, **64**(3), 281–288.

Zerihun Y. T. (2019) On steady two-dimensional free-surface flows with spatially-varied discharges, *Slovak J. Civ. Eng.*, **27**(3), 1–11.

Zerihun Y. T. (2020) Free flow and discharge characteristics of trapezoidal-shaped weirs, *Fluids*, **5**(4), doi:10.3390/fluids5040238.

Zerihun Y. T. (2021) Non-hydrostatic transitional open-channel flows from a supercritical to a subcritical state, *Slovak J. Civ. Eng.*, **29**(2), 39–48.

Zerihun Y. T. (2023) A study of the sedimentation and storage capacity depletion of a reservoir, *Slovak J. Civ. Eng.*, **31**(2), 37–47.